Strong lateral displacement in polarization anisotropic extraordinary transmission metamaterial

2010 New J. Phys. 12 063037

(http://iopscience.iop.org/1367-2630/12/6/063037)

New Journal of Physics
The open-access journal for physics

Strong lateral displacement in polarization anisotropic extraordinary transmission metamaterial

M Beruete[1], **M Navarro-Cía and M Sorolla**
Millimetre and Terahertz Waves Laboratory, Universidad Pública de Navarra, E-31006 Pamplona, Spain
E-mail: miguel.beruete@unavarra.es

New Journal of Physics **12** (2010) 063037 (15pp)
Received 15 March 2010
Published 30 June 2010
Online at http://www.njp.org/
doi:10.1088/1367-2630/12/6/063037

Abstract. In this paper, a deep numerical as well as experimental study of the anisotropy response of extraordinary transmission metamaterials constructed by stacking subwavelength hole arrays is presented. Two-dimensional (2D) dispersion diagrams for S- and P-polarization were obtained from simulation. From them, it was found that negative refraction can be obtained for the latter case for small angles of incidence. Additionally, it was found that double periodic and dielectric loaded hole arrays are optimal to enlarge the numerical aperture that leads to negative refraction. Several experiments are then presented in the V-band of the millimetre-wave range that show excellent agreement with the numerical calculations. Moreover, the richness of the anisotropic characteristic exhibited by the stacked hole array structure allows for designing structures with complex electromagnetic response other than solely negative refraction. Thus, the results presented here could be taken as a novel route to achieve exotic behaviour, such as negative refraction at other frequency ranges, like terahertz or the visible.

[1] Author to whom any correspondence should be addressed.

Contents

1. Introduction

Optical properties of natural crystals basically rely on electrical anisotropy, and, in general, their properties mainly depend on the direction of the electric field [1]. As a consequence, the index of refraction of crystals can take different values at different directions, and therefore their reciprocal space representation has the shape of three-dimensional (3D) ellipsoidal surfaces. A wide variety of propagation regimes can be obtained as a function of the values of the diagonal elements of the permittivity tensor.

With the advent of metamaterials more than a decade ago, a different viewpoint from which to explore material properties was introduced, which was a source of fresh ideas and revolutionary concepts. Previously, theories were based on microscopic (atomic) properties [2, 3], while composite and metamaterials use effective macroscopic parameters that may be arbitrarily exotic, although the physical meaning is sometimes unclear. The most intriguing property of metamaterials is the possibility of obtaining a negative index of refraction by double negativity, as was pointed out in the original work by Veselago [4], where he studied the electromagnetic properties of homogeneous and isotropic media having simultaneously negative values of dielectric permittivity and magnetic permeability. In that seminal paper, the inversion of Snell's law, as well as the reversion of the Doppler and Cerenkov effects, was deduced, and the ability of a planar slab with those characteristics to concentrate the rays emanating from a point source onto a focus was highlighted. Later, Pendry [5] extended this idea to evanescent modes, showing that they could be amplified by such a slab, giving as a result a perfect image reconstruction at the focal point. However, it was soon noticed that losses would introduce a penalty in the resolution of such a slab, fundamentally limiting its performance [6, 7]. Moreover, in practical applications, losses became an essential constraint for the development of optical metamaterials, motivating the progress of different techniques to obtain them with arrangements [8] alternative to the initial combination of wire and ring-resonator arrays [9] or exploiting surface plasmon polaritons [6, 7].

In addition, other studies were devoted to elucidate other means of achieving negative refraction, avoiding the strict constraint of having homogeneous negative values of permittivity and permeability [10, 11]. Needless to say, we are not considering the former strategy based on negative group velocity because of its principle of operation close to absorption resonances [5]. In [8], the concept of anisotropy was generalized comprising magnetic anisotropy, and from this it was established that negative refraction could happen in certain uniaxially anisotropic media.

Moreover, in [11] the concept was further extended to indefinite media and a classification into four groups was proposed: cut-off, anti-cut-off, always cut-off and never cut-off. Ellipsoidal and hyperbolic dispersion plots were obtained, depending on the relative sign of the diagonal components of both permittivity and permeability tensors. Later on, refraction laws of these materials and the behaviour under oblique incidence with respect to the crystal axes were comprehensively analysed [7, 12].

One of the most promising realizations of optical metamaterials is achieved by stacking metallic plates perforated with an array of apertures [13, 14]. In these structures, losses are still of concern and could be alleviated by designing properly the hole array to work at the extraordinary optical transmission (EOT) resonance, as we have in the millimetre-wave band in the past [15, 16]. The acronym EOT was coined more than a decade ago by Ebbesen *et al*, in a paper devoted to the experimental study of an unusually high transmittance peak, while working with metallic plates perforated with an array of small holes [17]. This was an appropriate denomination, since the peak occurred within the hole cut-off zone of the spectrum, where a very low transmission could, in principle, be expected. As the experiment was done in optics, the interpretation was made in terms of surface plasmon polaritons, but, subsequently, similar peaks were reported in other frequency ranges where metal models are closer to perfect conductors and, in consequence, plasmons cannot exist [18]. This initial discrepancy was finally clarified in [19] by observing that perforated plates support surface waves whose current distribution resembles that of surface plasmons in metals at optical frequencies. This type of surface wave has historically been identified as leaky waves, which exist in periodic structures and which, under the appropriate conditions, can give rise to the so-called resonant Wood anomalies [20]. In fact, in [21], EOT was explained invoking those resonances. Although mostly developed and known in the area of microwave engineering, leaky waves are not restricted to this frequency range. As a matter of fact, a comprehensive study of the influence of leaky waves on the optical properties of mesh gratings can be found in [22], and the fundamental physical operation described in that paper is in a wide sense very similar to posterior analyses of EOT resonance, even though the apertures in [22] were designed to work in propagation.

The design of metamaterials employing EOT plates in the millimetre-wave range has been an area of rapid development due to the comparatively easier fabrication and measurement techniques in this range as compared with devices operating in the visible. To date, we have been able to obtain miniaturized prototypes by employing double periodicity hole arrays backed with dielectric slabs [23], we have reported polarizers [24], we have proven negative refraction in a direct geometrical experiment using a prism [25], we have used this result to design lenses that enhance radiation of a point source [26] or translate the focal point to another focal point [27] and, closely related to the topic of this paper, we have demonstrated negative refraction through a bulk material with parallel faces (at difference with the prism) made of miniaturized EOT wafers [28].

In this paper, we extend the results of [28], and we show that the stacked hole array structure has a strongly anisotropic character and that its optical properties rely on the wave polarization and the angle of incidence. An initial study employing 2D dispersion diagrams serves as the starting point for the design of prototypes and permits us to envisage the possibility of achieving positive or negative refraction. The importance of dielectric slabs as well as a double periodic array is deduced from the numerical data and reasoned out based on theoretical results from the literature along with the numerical aperture concept. Then, measurement results are presented showing the beam displacement in each case, with good agreement with simulation results.

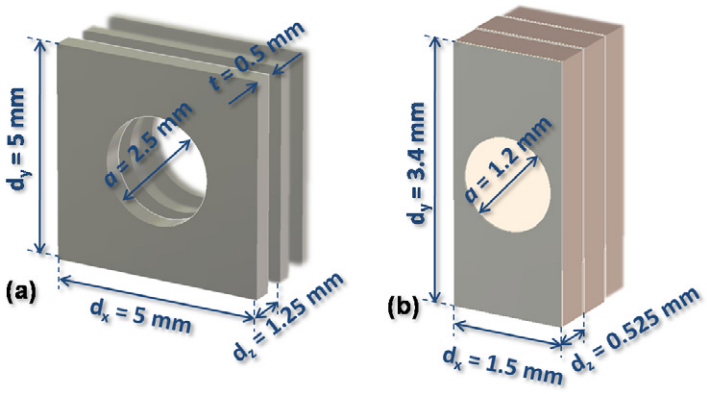

Figure 1. Unit cell of (a) free-standing and single periodic hole arrays and (b) dielectric loaded and double periodic hole arrays. In the latter case, dielectric height $h = 0.49$ mm and permittivity $\varepsilon = 2.43$.

2. Numerical analysis: two-dimensional (2D) dispersion diagrams

2.1. Free-standing and single period hole arrays

To begin with the numerical analysis, free-standing and square hole arrays were considered (see the unit cell in figure 1(a)). The structural parameters of this hole array are in-plane periodicities, $d_x = d_y = 5$ mm; longitudinal periodicity, $d_z = 1.25$ mm (this dimension is far below the half-wavelength); hole diameter, $a = 2.5$ mm; and metal thickness, $t = 0.5$ mm. With these dimensions, backward-wave propagation under normal incidence has already been reported in [15, 16]. As shown, a very small longitudinal periodicity was chosen in order to enhance the inter-plate electric coupling (series capacitance), according to the inverse transmission line model used in [15, 16] to explain the phenomenon. In fact, this is the smallest longitudinal periodicity we considered in previous experiments with free-standing stacked hole arrays [16] and should be optimal in terms of coupling, which is a key ingredient of backward-wave propagation.

The response of the infinite structure can be modelled with the commercial code CST Microwave Studio™ using a unit cell and imposing periodic boundary conditions in all dimensions. Then, by varying the phase difference between parallel periodic planes in two dimensions, the 2D dispersion diagrams can be calculated. The metal in the simulations is modelled as a perfect conductor, which is a reasonable approximation within the considered frequencies. Two distinct cases were considered, namely S- and P-polarization, and the results are shown in figures 2(a) and (b), respectively. Note that the axes show the wavevector components (tangential and normal) normalized to the periodicity along each axis (d_t and d_n, respectively; see the caption for more details).

To analyse the behaviour under each polarization, it is worth recalling that the refraction of the Poynting vector at the interface between a host medium (say air) and a finite stack of hole arrays can be obtained from the infinite medium band diagram by simply considering that (i) the tangential component of the wavevector must be conserved across the interface and (ii) the refracted wave must carry the energy away from the interface. The first condition forces identical k_t in both media and the second is equivalent to stating that the sign of the normal component of $\mathbf{v_g}(v_{gn})$ is conserved (the group velocity is the velocity of the energy flow inside the material

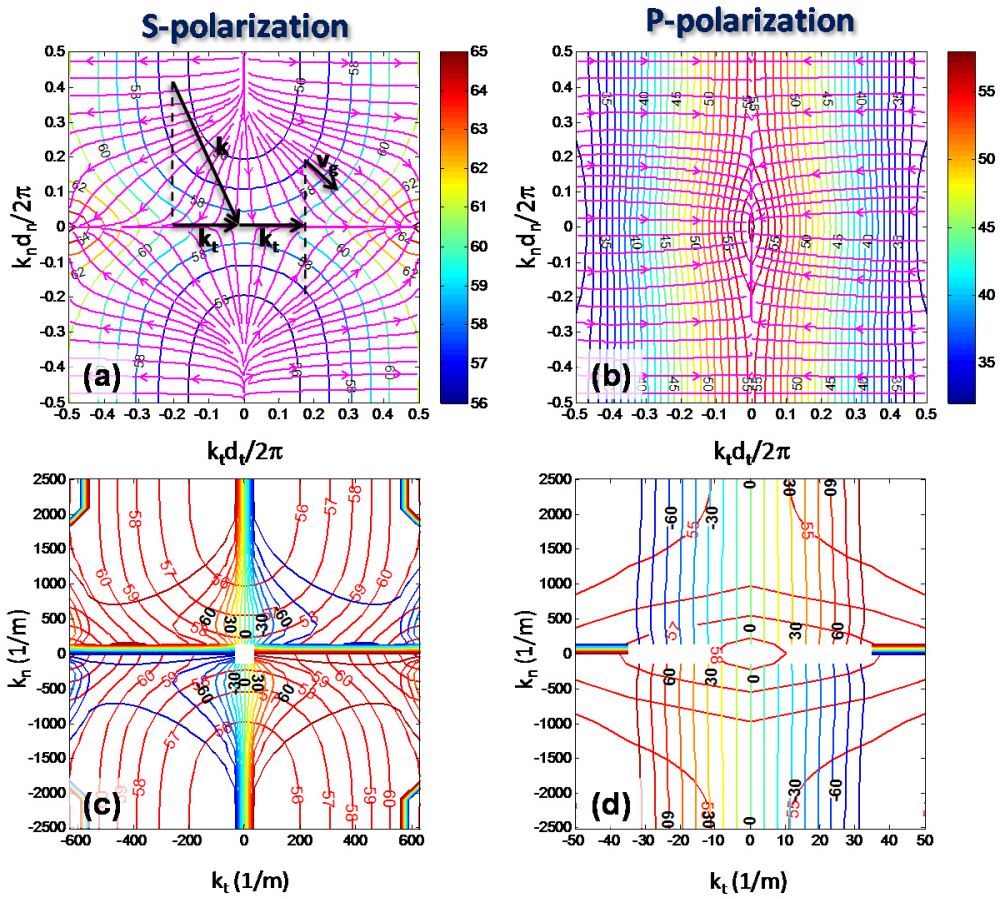

Figure 2. 2D dispersion diagrams and group velocity vectors (pink lines) of free-standing and single periodic hole arrays under S-polarization (a) and P-polarization (b). Iso-refraction angle curves mapped on the 2D dispersion diagrams under S-polarization (c) and P-polarization (d). (Note: d_n is the longitudinal periodicity, i.e. $d_n \equiv d_z = 1.25$ mm; d_t stands for tangential periodicity, i.e. $d_t \equiv d_x = d_y = 5$ mm.)

and, in general, is not parallel to the phase velocity). As explained in [11, 12], both phase and group velocities can be inferred from the 2D dispersion diagrams: phase velocity is inversely proportional to the wavevector, $\mathbf{v_p} = \omega/\mathbf{k}$, and group velocity is calculated as $\mathbf{v_g} = \nabla_\mathbf{k}\omega(\mathbf{k})$. As before, the group velocity is normalized and is represented in figures 2(a) and (b) as pink arrows, which, as expected, are orthogonal to the isofrequency curves.

An evident difference between S- and P-polarization is that in the former the band is shifted towards upper frequencies as the tangential wavevector is increased, and at the grazing angle the band takes place at 65 GHz. In contrast, under P-polarization the frequency decreases as the tangential wavevector is increased and, at the grazing angle, it is located at 34 GHz. The behaviour is also different in terms of refraction, as shown below. In fact, according to the nomenclature of [11], the stacked hole array structure under S-polarization behaves as a *never cut-off* medium with positive refraction, whereas under P-polarization it can be classified as a *cut-off* medium with negative refraction in the central part of the dispersion relation. This classification is only partially valid, since the shape of the isofrequency curves changes as k_t increases. For instance, for large enough k_t, the former case becomes more similar to a positive

refraction *anti-cut-off* medium, whereas in the latter case, the mode inside the structure becomes a trapped surface wave.

Under S-polarization, refraction is positive at all angles, although inside the structure, the normal components of the phase and group velocities have opposite signs, i.e. there is a backward wave in the longitudinal direction. The black arrows exemplify how to obtain the refracted angle from the diagram for an arbitrary oblique incidence at 57 GHz. First, conservation of k_t is applied and the wavevector is projected on the $f = 57$ GHz curves, yielding two possible solutions, the first and fourth quadrants. The application of the second condition fixes the solution that conserves the sign of the normal component of the group velocity. As the incident wave comes from a standard isotropic dielectric (air), $\mathbf{v_p}$ and $\mathbf{v_g}$ are identical and the sign of v_{gn} is negative. So, the valid solution is the one located at the first quadrant where the normal components of the wave and group velocities have opposite signs ($v_{pn} > 0$; $v_{gn} < 0$), whereas the transversal components have the same sign ($v_{pt} > 0$; $v_{gt} > 0$) inside the structure. Therefore refraction is positive, although there is backward propagation in the normal dimension, as mentioned above. From a qualitative analysis, it is also deduced that incidence at small angles leads to a small positive refraction, and as the angle is increased the angle of refraction also increases. Finally, for low frequencies, the refracted wave is nearly a surface wave (the tangential component dominates).

The mechanism is different for P-polarization (figure 2(d)). Applying a similar analysis as in the previous case, it can be inferred that for small angles of incidence there is a region where refraction is negative, and phase and group velocities have opposite signs in both their normal and their tangential components (an arrow plot has been omitted here for the sake of clarity, but the previous analysis is completely applicable). Then, as the angle of incidence increases, the mode practically becomes a trapped surface wave. So, interestingly, there is a narrow region where refraction is negative. In order to discern more clearly the numerical aperture of this region, figure 2(d) presents a detail of the 2D dispersion diagrams for denormalized wavevector components (red curves). Note that the normal component is much larger than the tangential component due to the shorter physical periodicity in that direction. Superimposed is the mapping of 'iso-refraction-angle' curves calculated through the relation

$$\theta_r = \arctan\left(v_{gt}/v_{gn}\right). \tag{1}$$

The 'iso-refraction-angle' curves are depicted as a rainbow coloured set with a step of 10°. The black number is the refraction angle inside the material calculated through (1) and it has been depicted with a step of 30°. From these curves it is readily observed that (i) refraction is negative from 55 to 58 GHz, with high refraction angles, and (ii) the coupled mode becomes a surface wave ($\theta_r > 90°$) when $k_t > 30\,\mathrm{m}^{-1}$ for any frequency (the figure is centred in the region of interest, but, as it can be deduced from figure 2(b), the group velocity is practically tangential out of the central zone). The numerical aperture can be calculated by the next equation:

$$\theta_i^{\max} = \arcsin\left(k_t^{\max}/k_0\right), \tag{2}$$

where k_0 is the wavevector in the first medium (air) and $k_t^{\max}$ is the largest tangential wavevector component coupled to a mode that is not a surface wave, in this case $k_t^{\max} = 30\,\mathrm{m}^{-1}$. Since the band is very narrow, the analysis can be particularized to the central frequency, 56.5 GHz, and from here a tiny numerical aperture of NA = 2.9° (±1.45°) is obtained. For the sake of completeness, the calculated numerical aperture under S-polarization is NA = 29° (obtained by applying (2) and considering, from figure 2(c), $k_t^{\max} = 300\,\mathrm{m}^{-1}$).

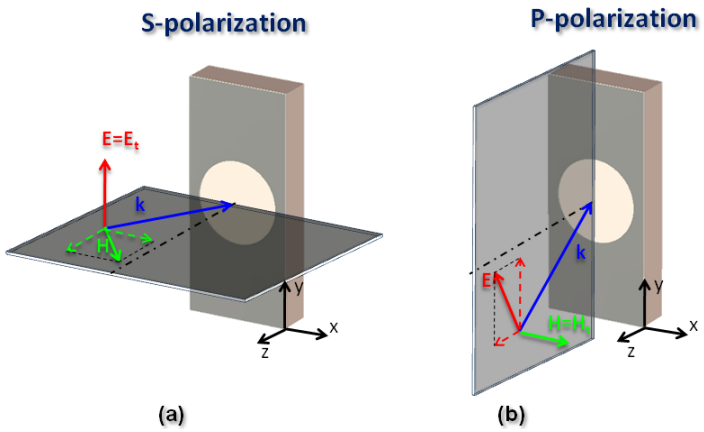

Figure 3. Schematic diagram showing the configuration under S-polarization (a) and P-polarization (b) for dielectric loaded and double periodic hole arrays. Note that the electric field must have a transversal component parallel to the large hole periodicity to excite EOT.

2.2. Dielectric loaded and double periodic hole arrays

The previously calculated numerical aperture to obtain negative refraction is very narrow and makes it very difficult to measure negative beam shift in practice. In order to increase the numerical aperture, two modifications can be introduced, as we did in [23]: (i) to embed the hole array between dielectric slabs and (ii) to use a hole array with double periodicity to increase the fractional aperture area and improve the transmission. The unit cell is shown in figure 1(b), along with the important parameters, which are in-plane periodicities, $d_x = 1.5\,\text{mm}$, $d_y = 3.4\,\text{mm}$; longitudinal periodicity, $d_z = 0.525\,\text{mm}$ (again, this dimension is far below the half-wavelength); hole diameter, $a = 1.2\,\text{mm}$; metal thickness, $t = 0.035\,\text{mm}$; dielectric height, $h = 0.49\,\text{mm}$; and relative permittivity, $\varepsilon_\text{r} = 2.43$. With these parameters, backward-wave propagation under normal incidence was reported in [23]. Moreover, in our previous work dealing with oblique incidence [28], we measured negative refraction under P-polarization, so this numerical study is focused on shedding more light to explain those results and, additionally, to analyse the S-polarization incidence.

Now the hole array is not symmetric and the exact meaning of S- and P-polarization must be clarified. First, it must be noted that, in order to excite regular EOT, the electric field must have a component parallel to the large hole array periodicity. So, under S-polarization (figure 3(a)), the plane of incidence must be the xz-plane and the field components are $E_\text{t} = E_y$, $H_\text{t} = H_x$ and $H_\text{n} = H_z$, where the subscripts 't' and 'n' refer to transversal and normal, respectively. On the other hand, under P-polarization (figure 3(b)), the plane of incidence is the yz-plane and the field components are $E_\text{t} = E_y$, $E_\text{n} = E_z$ and $H_\text{t} = H_x$. With these conditions, the transversal electric field is properly directed along y, allowing for the excitation of regular EOT resonance.

As before, the 2D dispersion diagrams are calculated and the results are shown in figures 4(a) and (b) for S- and P-polarization, respectively. The plots obtained are similar to their counterparts of free-standing and single period hole arrays, but, in general, the frequency span is larger in the present case. Under S-polarization the band extends from 50 GHz at normal incidence to 85 GHz at grazing, whereas under P-polarization the frequency decreases down to

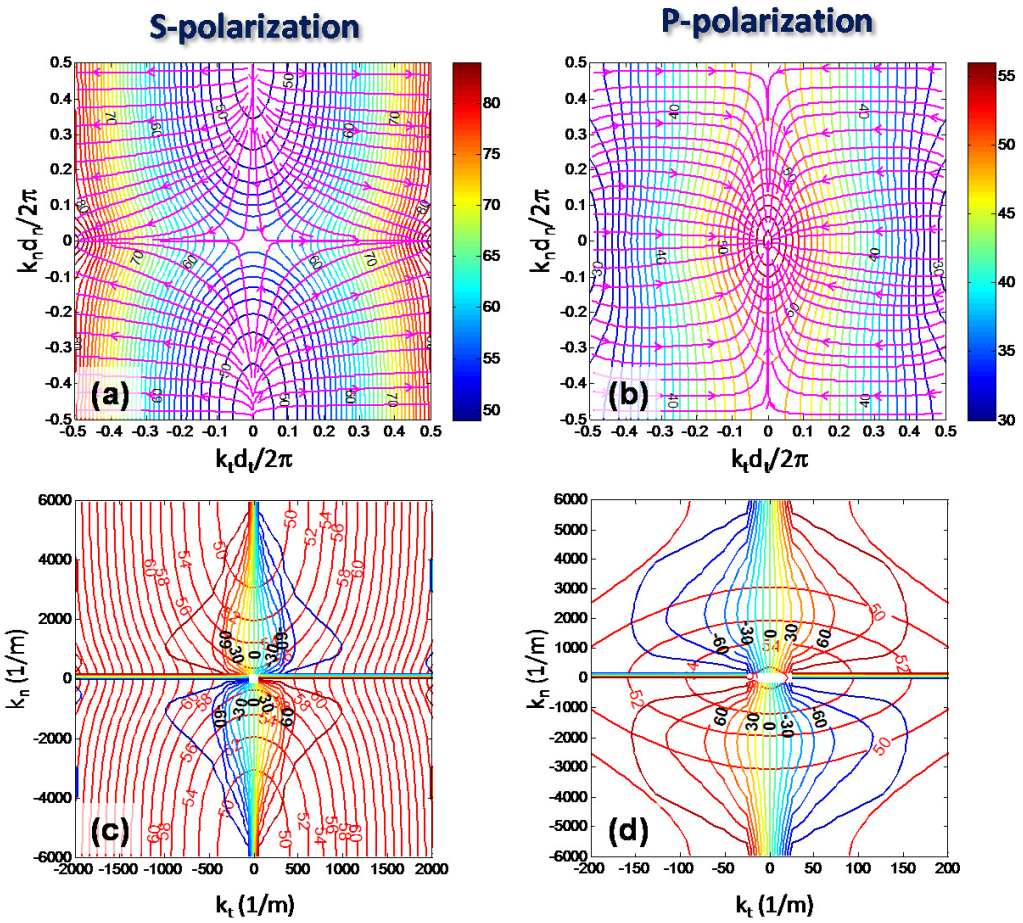

Figure 4. 2D dispersion diagrams and group velocity vectors (pink lines) of dielectric loaded and double periodic hole arrays under S-polarization (a) and P-polarization (b). Iso-refraction angle curves mapped on the 2D dispersion diagrams under S-polarization (c) and P-polarization (d). (Note: d_n is the longitudinal periodicity, i.e. $d_n \equiv d_z = 0.525$ mm; d_t stands for tangential periodicity, i.e. $d_t \equiv d_x = 1.5$ mm under S-polarization and $d_t \equiv d_y = 3.4$ mm under P-polarization.)

30 GHz at grazing incidence. Apart from this, the features under S-polarization are almost the same as in the previous section: there is positive refraction and backwards propagation along the normal component for all angles of incidence, the refraction angle increases with the incidence angle, and for large angles of incidence a surface wave appears on the structure.

It is more interesting to analyse P-polarization. It is readily seen in figure 4(b) that the negative refraction region is wider than before. Nevertheless, it is again surrounded by a region where the structure only supports surface waves. In parallel with the previous analysis, the numerical aperture (NA) to obtain negative refraction can be calculated from the 'iso-refraction-angle' curves of figure 4(d) and equation (2). Recognizing that $k_t^{max} = 150\,m^{-1}$ and that the band extends from 50 to 60 GHz, and particularizing the calculation to the central frequency, the resulting NA is 15° (±7.5°). Under S-polarization, NA = 80°(±40°). In this case, the value of k_t^{max} is not clear from the plot of figure 4(c), since it is highly divergent. As a compromise, a value of $k_t^{max} = 750\,m^{-1}$ has been chosen.

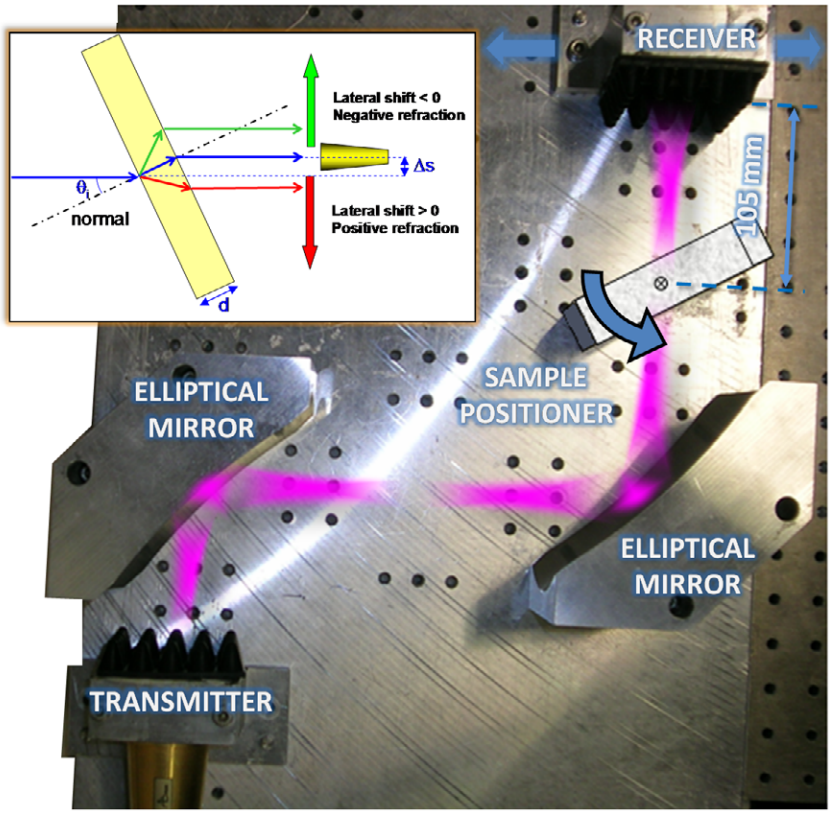

Figure 5. The experimental set-up and a schematic diagram showing the measurement procedure (inset).

Note that, by simply adding dielectric slabs to the single periodic hole array analysed in the previous section, the NA would increase, since the 2D dispersion diagram would be the same except for the frequency values that would decrease proportionally to $\varepsilon^{-1/2}$. Applying (2) again with $k_0' = k_0/\varepsilon^{1/2}$, the NA for a dielectric with relative permittivity $\varepsilon_r = 2.43$ under P-polarization would be 4.5° ($\pm 2.25^\circ$), which is a modest increment. So, the addition of double periodicity is vital to obtain a reasonable NA and, from that, a measurable negative refraction. This will be analysed in section 4.

3. Experimental results

After the numerical analysis, measurements were carried out within the V-band of the millimetre-wave spectrum. Some initial measurements were taken with free-standing, single periodic hole arrays to check that negative refraction was impossible to detect in any case (not included here).

Therefore, the experiment was focused on dielectric loaded and double periodic hole array wafers (see [23] or [28] for a picture of the prototypes), using one and four stacked layers for comparison purposes. The experimental setup is shown in figure 5. For S/P measurements, a horizontally/vertically polarized pure Gaussian beam [29] was generated by a transmitting corrugated horn antenna (Tx)—the polarization of the incident wave is modified because, as mentioned above, the electric field must have a transversal component parallel to the large hole

array periodicity to excite regular EOT and, for simplicity in the experimental procedure, the wafers are always tilted with respect to the reference plane given by the floor. This beam propagates up to a pair of focusing elliptical mirrors (A–B) designed to obtain an undistorted beam having its beam waist midway between the mirrors, where the sample is located. The sample is tilted at angles of 0°, 5°, 10°, 20° and 30° to observe the effect on the transmitted power. Finally, lateral power distribution at the output is scanned with another corrugated horn antenna located at 105 mm with a step of 5 mm. The spectra extend from 50 to 72 GHz and are registered with an ABmm Millimetre Wave Vector Analyzer. The measurements thus made are depicted in figures 6 and 7 for one and four plates, respectively. Note that P-polarization results have already been published in [28] and that they have been included here for the sake of completeness and in order to make easier the comparison between S- and P-polarization, which is of primary interest in this work. In the figures, the vertical axes display the displacement of the receiving antenna from the central position and the horizontal axes show the frequency range. The point of zero displacement corresponds to the position where the refracted ray would emerge if $n = 0$ inside, that is, assuming that the refracted ray inside the structure is parallel to the normal.

When a single wafer is introduced in the quasi-optical bench and under normal incidence, a clear frequency filtering effect is obtained within the ET band for both S- and P-polarization (actually, under normal incidence they should be identical) around 65 and 71 GHz, in good agreement with the results of [23]. Increasing the angle of incidence to $\theta_i = 5°$ has almost no effect for S-polarization, whereas for P-polarization the beam progresses slightly towards negative values. The frequency filtering is also present, and the band remains approximately within the above-mentioned frequencies. An increment to $\theta_i = 10°$ moves the beam towards positive values and increases the frequency for S-polarization. In contrast, the negative displacement is emphasized and the frequency band is shifted downwards for P-polarization. Notice also that, in the latter, the peak amplitude diminishes somewhat but still has an appreciable level. At the incidence angle of $\theta_i = 20°$, the tendency is the same: positive/negative frequency and beam shift for S-/P-polarization. Also, for P-polarization a second band emerges at around 71 GHz with no apparent lateral shift. Finally, when $\theta_i = 30°$, the results show the typical trend but the magnitude of the first band decreases for P-polarization. The aforementioned second band is also shifted downwards in frequency with a negligible lateral shift.

When four wafers are stacked (figure 7), the measurement under normal incidence shows a frequency filtering with the ET band located around 54.6 GHz (see again [23]). In fact, the plots under S- and P-polarization are somewhat different, probably due to misalignment or some experimental error. Due to losses (we are employing a microwave substrate for the prototypes designed at the millimetre-wave range), the peak level in this case is around −15 dB, a moderately high value. When $\theta_i = 5°$, the ET band maintains its position in frequency in both cases. Very interestingly, for S-polarization, no appreciable beam shift is observed, whereas a clear negative beam shift of approximately 5 mm ($\sim\lambda$) appears. In the case of $\theta_i = 10°$, the band remains within the same frequencies for S-polarization and a tiny positive beam shift is recorded. On the other hand, for P-polarization, the band downshifts to 54.2 GHz with a strong lateral beam displacement of around 20 mm. When $\theta_i = 20°$, the positive beam shift is clearly augmented under S-polarization and a slight shift towards upper frequencies is perceived, along with some reduction in its magnitude. A very important result is that, for P-polarization, transmission is abruptly destroyed, indicating that a critical angle has been exceeded. Finally, at $\theta_i = 30°$, the tendency for S-polarization is maintained, with positive beam and frequency shifts, whereas for P-polarization, transmission is completely annihilated.

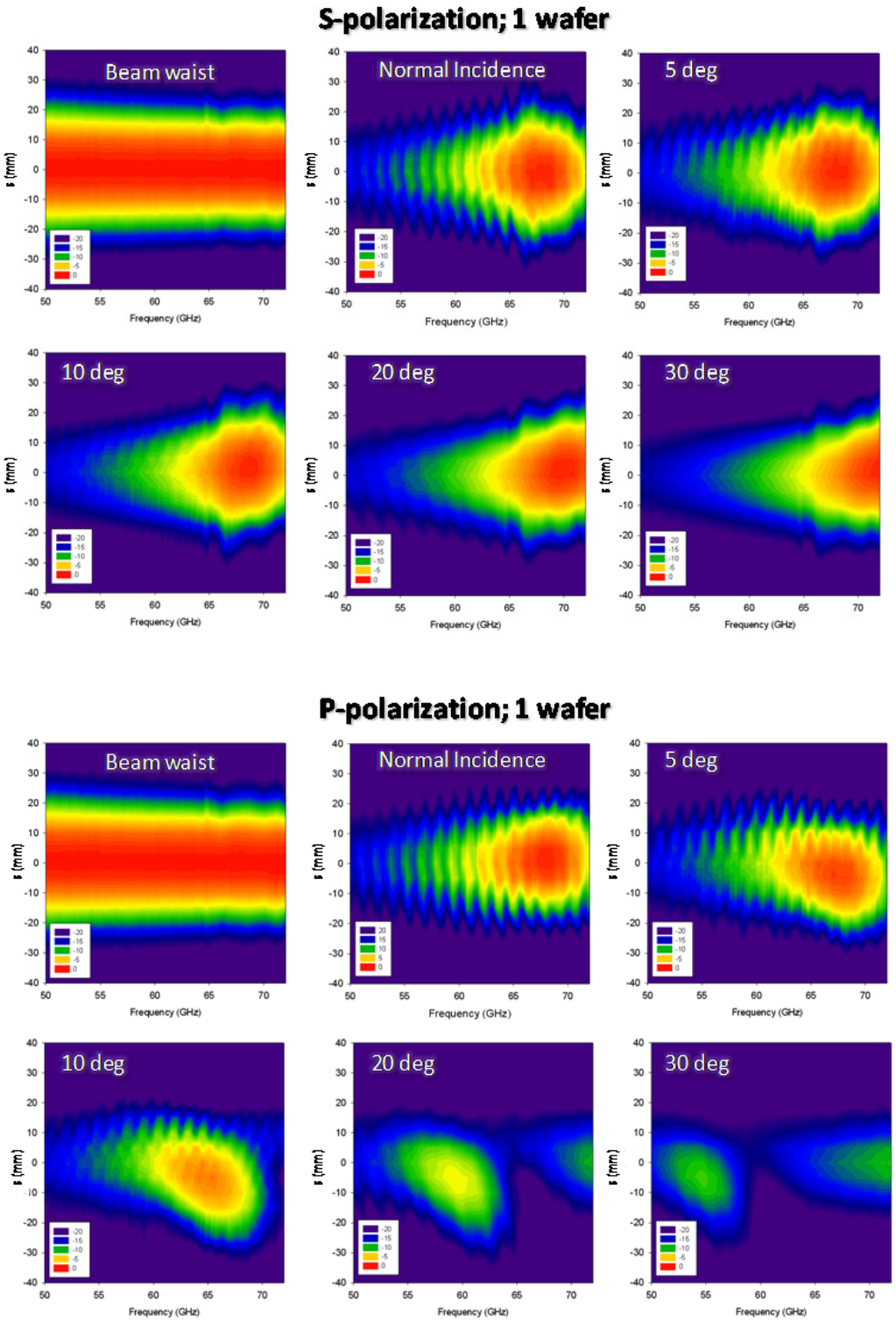

Figure 6. Measurement results for one single wafer under S- (above) and P-polarization (below) and several angles of incidence. Frequency is in abscissas and beam shift in ordinates.

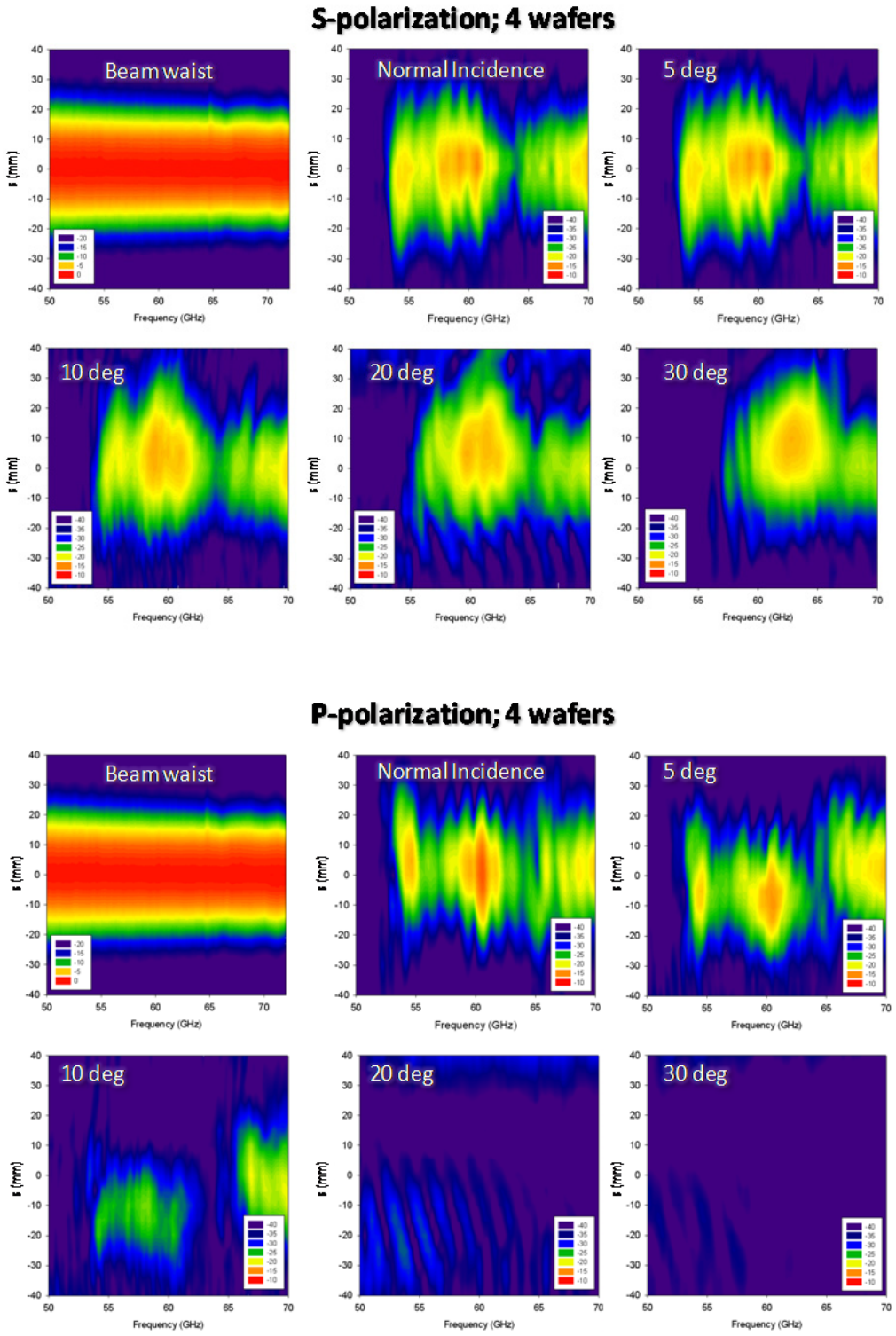

Figure 7. Measurement results for four stacked wafers under S- (above) and P-polarization (below) and several angles of incidence. Frequency is in abscissas and beam shift in ordinates.

4. Discussion and comparison between simulation and experimental results

From the previous analysis of the experimental results, there is evidently good qualitative agreement with the numerical calculations of figure 4: refraction is positive under S-polarization and there is a clear negative refraction for some angles under P-polarization incidence. Moreover, the experimental numerical aperture is larger for S-polarization than for P-polarization, as predicted from the simulation.

Very interestingly, clear beam shifts were observed even for single wafer measurement, being positive and negative for S- and P-polarization, respectively. In principle, these results cannot be explained through the isofrequency curves of the bulk material, so the beam shift must be understood as a direct effect of the excited leaky waves responsible for the EOT resonance. The leaky wave runs along the perforated plate perpendicular to the magnetic field and, as discussed in [22], is a backward-wave mode (otherwise it would be an improper wave [30]). From here, the phase difference between holes is negative under P-polarization and then the beam is negatively shifted. Under S-polarization, the leaky wave runs orthogonal to the plane of incidence, so it does not introduce an additional phase and, in principle, no shift, or at most a tiny positive shift, can be expected.

Next, let us check if the experiment and simulation agree quantitatively as well. First, it is noticed that the frequency band in the experiment appears slightly shifted upwards with respect to simulation. This may be due to the presence of a small adhesive layer in the experiment or, more probably, to a strong mismatch between the incident Gaussian beam and the mode inside the structure at the band edge. Indeed, the results for one wafer show that the band starts at 50 GHz, so the agreement can be considered good.

As for the NA in each case, we found from the simulation that under S-polarization the NA is approximately $\pm 40^\circ$, and under P-polarization it is $\pm 7.5^\circ$, whereas in the experiment we found that under P-polarization and around 10° the transmission decreased rapidly, and for S-polarization we obtained decent transmission even for the largest measured angle of 30°. So, again the agreement is quantitatively good. The fact that in the P-polarization experiment we still recorded transmission even at 10° when the cut-off should be at 7.5° may be due to the intrinsic finiteness of our structure. Indeed, we employ a thin slab of 2.59 mm ($\sim 0.7\lambda$ at the frequency of interest, considering dielectric of $\varepsilon_r = 2.43$) and power can be coupled to the output, even though the infinite dispersion diagram predicts an almost surface wave with that angle. Moreover, this explains the relatively high value of the beam shift: around -20 mm (the maximum is up to -30 mm!). The lateral beam shift can be calculated as (see the inset of figure 5.)

$$\theta_r = \arctan\left(\frac{s}{d\cos(\theta_i)}\right), \tag{3}$$

where s is the lateral beam shift, d the total stack thickness, θ_i the angle of incidence and θ_r the angle of refraction. From the expression, we can deduce a value of $\theta_r = -82^\circ$ for the experimental conditions ($\theta_i = 10^\circ$, $d = 2.59$ mm and $s = -20$ mm). This is in excellent agreement with the strong divergence observed in figures 4(b) and (d), where the angle of refraction approaches 90°. This also explains why, when the angle of incidence exceeds 10°, the transmittance is abruptly obliterated. Obviously at 20° and 30° the incident Gaussian beam is much more efficiently and strongly coupled to a trapped surface wave, and power runs along the structure until it vanishes due to ohmic losses and/or is radiated on the edges.

As for S-polarization, a beam shift of around 10 mm is observed in figure 7 when the angle of incidence is 30°. If (3) is applied with those parameters ($\theta_i = 30^\circ$, $d = 2.59$ mm and

$s = 10\,\text{mm}$), a value of $\theta_r = 77^\circ$ is obtained. This is again in excellent agreement with the divergence observed in the isofrequency curves of figures 4(a) and (c). Note that in this case, in the 'iso-refraction-angle' curves there is an abrupt change around 80°, but for smaller refraction angles the curves change more gently. This explains why the experimental power distribution has a less marked dependence on the frequency and position.

There is still an aspect that should be clarified. As shown, the cornerstone to widen the numerical aperture is the use of a rectangular unit cell (the dielectric loading also helps but the main role is played by the double period). The explanation can be found using an equivalent circuit model. As we discussed in [15], an extraordinary transmission hole array at resonance can be modelled as an L-C tank. So, if the periodicity is reduced in one dimension (the cell moves from square to rectangular), magnetic flux across the holes increases and, therefore, self-inductance also increases, leading to a reduction in the resonance frequency. Then, applying (2), it is clear that the numerical aperture should increase: for the same tangential wavevector, the frequency and free-space wavenumber decrease.

5. Conclusions

In summary, in this paper we presented an in-depth analysis of the rich anisotropic characteristics of extraordinary transmission metamaterials made by stacking extraordinary transmission hole arrays. First, a comprehensive numerical study focused on the 2D dispersion diagrams of free-standing and single periodic stacked hole arrays under S- and P-polarization incidence was carried out. It was shown that under S-polarization the medium always has positive refraction and behaves like a *never-cut-off* or *anti-cut-off* medium for small or large angles, respectively. On the other hand, under P-polarization the medium features a *cut-off* characteristic with negative refraction for short angles, and beyond an angle it supports a surface wave.

It was demonstrated that the NA with P-polarization is much smaller than that with S-polarization and, for free-standing and single periodic stacked hole arrays, that it leads to an impractically narrow NA that makes it difficult, if not impossible, to measure negative refraction.

In general, the NA can be widened by employing double periodic and dielectric loaded hole arrays. This has been analysed with an equivalent circuit approach. The calculations performed showed that a measurable negative refraction could be achieved by embedding the hole arrays in slabs of relatively low dielectric permittivity, but, in order to enhance significantly the NA, double periodicity is crucial. Afterwards, experiments for one and four stacked wafers under S- and P-polarization in the millimetre-wave range demonstrated clearly the features observed in the numerical computations. The shift observed for one wafer can be explained by invoking the leaky wave model, which explains EOT resonance. The study with four wafers has been correlated with the numerical results and the observed beam shifts agree excellently with the simulation.

The presented results could open the way to designing negative refraction structures based on stacked hole arrays. The NA could be further increased by employing higher-permittivity dielectric materials. However, losses may increase. Moreover, the richness of the dispersion diagram allows for the design of structures with complex response without being restricted to negative refraction. Currently, it is indisputable that EOT takes place in every region of the electromagnetic spectrum, regardless of the interpretation given to explain the phenomenon, and therefore the results presented here could be downscaled to other frequency ranges that are more interesting from a technological viewpoint, such as terahertz or even the visible.

Acknowledgments

This work was supported by the Spanish Government under the contract Consolider 'Engineering Metamaterials' CSD2008-00066.

References

[1] Born M and Wolf E 1999 *Principles of Optics* (Cambridge: Cambridge University Press)
[2] Jackson J D 1999 *Classical Electrodynamics* (New York: Wiley)
[3] Kong J A 2008 *Electromagnetic Wave Theory* (Cambridge, MA: EMW Publishing)
[4] Veselago V G 1968 *Sov. Phys.—Usp.* **10** 509
[5] Pendry J B 2000 *Phys. Rev. Lett.* **85** 3966
[6] Solymar L and Shamonina E 2009 *Waves in Metamaterials* (New York: Oxford University Press)
[7] Ramamrishna S A and Grzegorczyk T M 2009 *Physics and Applications of Negative Refractive Index Material* (Boca Raton, FL: CRC Press)
[8] Shalaev V M 2007 *Nat. Photon.* **1** 41
[9] Smith D R, Padilla W J, Vier D C, Nemat-Nasser S C and Schultz S 2000 *Phys. Rev. Lett.* **84** 4184
[10] Lindell I V, Tretyakov S A, Nikoskinen K I and Ilvonen S 2001 *Microw. Opt. Technol. Lett.* **31** 129
[11] Smith D R and Schurig D 2003 *Phys. Rev. Lett.* **90** 077405
[12] Grzegorczyk T M, Nikku M, Chen X, Wu B-I and Kong J A 2005 *IEEE Trans. Microw. Theory Tech.* **53** 1443
[13] Zhang S, Fan W, Panoiu N C, Malloy K J, Osgood R M and Brueck S R J 2005 *Phys. Rev. Lett.* **95** 137404
[14] Dolling G, Enkrich C, Wegener M, Soukoulis C M and Linden S 2006 *Science* **312** 892
[15] Beruete M, Sorolla M and Campillo I 2006 *Opt. Express* **14** 5445
[16] Beruete M, Campillo I, Navarro-Cía M, Falcone F and Sorolla Ayza M 2007 *IEEE Trans. Antennas Propag.* **55** 1514
[17] Ebbesen T W, Lezec H J, Ghaemi H, Thio T and Wolf P A 1998 *Nature* **391** 667
[18] Beruete M, Sorolla M, Campillo I, Dolado J S, Martín-Moreno L, Bravo-Abad J and García-Vidal F J 2004 *Opt. Lett.* **29** 2500
[19] Pendry J B, Martín-Moreno L and García-Vidal F J 2004 *Science* **305** 847
[20] Hessel A and Oliner A A 1965 *Appl. Opt.* **4** 1275
[21] Sarrazin M, Vigneron J P and Vigoureux J M 2003 *Phys. Rev.* B **67** 085415
[22] Ulrich R 1974 *Proc. Symposium on Optical and Acoustical Micro-Electronics* (*Microwave Research Institute Symposium Series* vol 23) ed J Fox (New York: Polytechnic Press of the Polytechnic Institute of New York) pp 359–76
[23] Beruete M, Sorolla M, Navarro-Cía M, Falcone F, Campillo I and Lomakin V 2007 *Opt. Express* **15** 1107
[24] Beruete M, Navarro-Cía M, Sorolla M and Campillo I 2007 *Opt. Express* **15** 8125
[25] Navarro-Cía M, Beruete M, Sorolla M and Campillo I 2008 *Opt. Express* **16** 560
[26] Beruete M, Navarro-Cía M, Sorolla M and Campillo I 2008 *Opt. Express* **16** 9677
[27] Navarro-Cía M, Beruete M, Sorolla M and Campillo I 2009 *Appl. Phys. Lett.* **94** 144107
[28] Beruete M, Navarro-Cía M, Sorolla M and Campillo I 2009 *Phys. Rev* B **79** 195107
[29] Goldsmith P F 1998 *Quasioptical Systems—Gaussian Beam, Quasioptical Propagation and Applications* (Piscataway, NJ: IEEE Press)
[30] Ishimaru A 1990 *Electromagnetic Wave Propagation, Radiation, and Scattering* (Englewood Cliffs, NJ: Prentice-Hall)